Weather and Climate Extremes 47 (2025) 100756

Contents lists available at ScienceDirect

Weather and Climate Extremes

journal homepage: www.elsevier.com/locate/wace

Quantifying moisture and sensible heat flux anomalies for compound drought and heat wave events in the Iberian Peninsula

Albenis Pérez-Alarcón [a,b,c,*], Marta Vázquez [a], Alexandre M. Ramos [d], Raquel Nieto [a,e], Joaquim G. Pinto [d], Luis Gimeno [a,e]

[a] Centro de Investigación Mariña, Universidade de Vigo, Environmental Physics Laboratory (EPhysLab), Campus As Lagoas s/n, 32004, Ourense, Spain
[b] Instituto Dom Luiz (IDL), Faculdade de Ciências, Universidade de Lisboa, 1749-016, Lisboa, Portugal
[c] Departamento de Meteorología, Instituto Superior de Tecnologías y Ciencias Aplicadas, Universidad de La Habana, 10400, La Habana, Cuba
[d] Institute of Meteorology and Climate Research Troposphere Research (IMKTRO), Karlsruhe Institute of Technology (KIT), Karlsruhe, Germany
[e] Galicia Supercomputing Center (CESGA), Santiago de Compostela, Spain

ARTICLE INFO

Keywords:
Moisture sources
Heat sources
Droughts
Heat waves
Lagrangian analysis
Iberian Peninsula
Compound event

ABSTRACT

Compound drought and heat wave events (CDHWs) are weather and climate hazards whose frequency is increasing in many regions across the globe. Here, we applied a novel Lagrangian atmospheric moisture and heat tracking framework to the outputs of the Lagrangian FLEXPART model driven by the ERA5 reanalysis to quantify the moisture and sensible heat flux anomalies for CDHWs occurred in the Iberian Peninsula in the extended summer (May–October) from 1991 to 2022. CDHWs are identified based on the 95th percentile of daily maximum and minimum temperatures and the self-calibrating Effective Drought Index. The Lagrangian framework is then applied to the top 20 CDHWs affecting more than 50% of continental Iberian Peninsula. Our analysis reveals that these events endure on average 10.35 days, with 2022 achieving the highest number of days (46 days) under dry and hot conditions. CDHW events are generally associated with blocking situations and high-pressure systems, whose effects can be amplified by the local land-atmosphere feedback. The results indicate that the Iberian Peninsula itself is the principal moisture source for the low summertime precipitation, followed by the North Atlantic Ocean corridor and the western Mediterranean Sea, but their total moisture contribution decreases by about 56% during the CDHWs. Moreover, the sensible heat sources pattern exhibits a local-to-regional origin, with ~35% above the climatological value during the dry and hot events. Overall, this study provides new insight into the underlying mechanisms of CDHWs, which could be useful for helping in understanding these events in the context of global warming.

1. Introduction

There is a very wide agreement that global warming can alter weather and climate variability on global, regional, and local scales (IPCC, 2021). In particular, global warming may intensify the frequency and severity of extreme weather phenomena, e.g., droughts and heat waves, which will have more noticeable impacts on the Earth system in the future (e.g., Barriopedro et al., 2011; Perkins-Kirkpatrick and Lewis, 2020; Zscheischler et al., 2020). For instance, droughts and heat waves often result from the interactions of several physical processes, achieving more significant impacts when they occur as a compound event rather than a single event (Zscheischler et al., 2018). Such compound drought and heat wave events (hereafter CDHWs) have received more attention in recent years due to their increasing frequency in many regions across the globe and their major implications for social-ecological systems (Chen et al., 2019; Zhang et al., 2019; Mukherjee et al., 2020; Sutanto et al., 2020; Wang et al., 2021; Rousi et al., 2023). These events exacerbated by climate change affect agriculture, water availability and public health (Neumann et al., 2017; Lloret and Kitzberger, 2018; Barichivich et al., 2019; Brás et al., 2021; Knutzen et al., 2025). Prolonged droughts intensify water resource scarcity, reducing agricultural productivity and increasing wildfire risk (e.g., Kuwayama et al., 2019; Venkatappa et al., 2021). Furthermore, extreme heat waves can cause thermal stress and even mortality in

* Corresponding author. Centro de Investigación Mariña, Universidade de Vigo, Environmental Physics Laboratory (EPhysLab), Campus As Lagoas s/n, 32004, Ourense, Spain.
E-mail address: albenis.perez.alarcon@uvigo.es (A. Pérez-Alarcón).

https://doi.org/10.1016/j.wace.2025.100756
Received 6 July 2024; Received in revised form 29 January 2025; Accepted 16 February 2025
Available online 17 February 2025

humans and animals (e.g., Perkins-Kirkpatrick and Lewis, 2020; García-León et al., 2021; Salvador et al., 2023).

Previous studies have extensively documented past extreme droughts and heat waves in different regions around the world. For example, the summers of 2003, 2010, 2015, 2017, 2018, and 2022 achieved not only extreme droughts but also numerous heat-related deaths and extensive forest fires in west-central Europe and west Russia (Christensen and Christensen, 2003; Fink et al., 2004; Barriopedro et al., 2011; Hauser et al., 2016; Turco et al., 2017; Hao et al., 2020; Molina et al., 2020; Tripathy and Mishra, 2023; Ramos et al., 2023). Additionally, several works (e.g., Russo et al., 2015, 2019; Sánchez-Benítez et al., 2018, 2020; Tripathy and Mishra, 2023) have pointed out that Euro-Mediterranean droughts and heat waves are becoming more frequent and intense, being the Iberian Peninsula (IP) one of the most affected areas (Russo et al., 2019; Tripathy and Mishra, 2023). Indeed, future projections for the IP reveal an increase in water scarcity and frequency of more severe drought episodes (Ojeda et al., 2021; Moemken et al., 2022; Alvarez et al., 2024) and high extreme temperatures (Molina et al., 2020; Carvalho et al., 2021; Lorenzo et al., 2021).

While there are several different definitions for droughts, they can be generally seen as prolonged periods of precipitation shortage, frequently caused by precipitation deficits or high evaporative demand and can extend from several months to years or decades (Vicente-Serrano et al., 2020; Zhang et al., 2022). In addition, heat waves in the European region are extremely high temperatures events often linked to the influence of atmospheric blocking situations linked to high-pressure, anticyclonic surface systems, which may last from days to weeks and induce extreme events (Di Luca et al., 2020; Kautz et al., 2022; Hao et al., 2022). The predictability of blocking situations remains a challenge (e.g. Quandt et al., 2019), and thus the predictive skill to determine the onset and evolution of droughts and heat waves remains limited. However, it is widely accepted that CDHWs are frequently triggered by anomalies in local land-atmospheric (Santanello et al., 2017; Miralles et al., 2019; Barriopedro et al., 2023) and in the large-scale atmospheric and oceanic circulations (Hao et al., 2018). Overall, from the thermodynamic framework, heat waves result from temperature advection (e.g., Garfinkel and Harnik, 2017; Tamarin--Brodsky et al., 2020), adiabatic compression (e.g., Bieli et al., 2015; Zschenderlein et al., 2019) and diabatic heating through surface sensible heat fluxes (e.g., Miralles et al., 2019; Zhou and Yuan, 2022).

Geographical regions under CDHWs can be characterized by atmospheric blocking situations, with downward large-scale winds suppressing cloudiness, and reduced moisture in the lower atmosphere (e.g., Mukherjee et al., 2020; Kautz et al., 2022). While the thermodynamic processes associated with heat waves and drought events are to a large extent known, there is limited understanding in terms of dynamical aspects, different regional forcings and feedbacks (e.g., Barriopedro et al., 2023; Rousi et al., 2023). In general terms, the large-scale and regional conditions result in enhanced evapotranspiration (Liu et al., 2015; Miralles et al., 2019). Furthermore, the limited moisture availability during a CDHW event hinders evaporative cooling, limiting latent heat fluxes over land surfaces (Berg et al., 2014). Typically, this would lead in turn to an amplification of preexisting hot and dry conditions through further increasing diabatic heating (Stéfanon et al., 2014). Therefore, CDHW events are also characterized by anomalies in the surface energy budget. However, which source regions exhibit negative anomalies in moisture support and above-average sensible heat contributions during these extreme events remains an open question.

Lagrangian moisture tracking methods have been extensively used to identify moisture sources for precipitation events in many regions of the world (see Gimeno et al., 2020; and references therein) and for highly precipitating weather systems, such as cyclones (e.g., Papritz et al., 2021; Pérez-Alarcón et al., 2022, 2023) and atmospheric rivers (e.g., Ramos et al., 2016; Algarra et al., 2020). Lagrangian trajectories provide a picture of source regions, typical transport patterns, and physical processes in the air masses for temperature extremes (Bieli et al., 2015; Santos et al., 2015; Zschenderlein et al., 2018). Following this approach, Schumacher et al. (2019) identified heat sources for mega heat waves, and Schumacher et al. (2020) showed the advantages of a combined diagnosis of heat and moisture source regions to understand dry and hot conditions during compound events. Recently, Li et al. (2024) performed a combined Lagrangian moisture and heat sources analysis to investigate the occurrence of yield deficits over the largest rainfed wheat belt in Australia, while Zhou et al. (2024) followed the heat tracking approach from Schumacher et al. (2019) to investigate connection between upwind droughts and heat waves over East China.

Given the disastrous impacts of CDHWs and the need for an improved understanding of this extreme under global warming, the aim of this study is to utilize a novel Lagrangian framework to trace the origins of sensible heat and moisture for quantifying moisture and sensible heat flux anomalies during the CDHW events that occurred in the IP from 1991 to 2022. The remainder of this paper describes data and methods in Section 2 to identify CDHW events in the IP and the Lagrangian moisture and sensible heat sources identification. Results and discussion are presented in Section 3, while Section 4 summarizes the main findings and describes plans for future works.

2. Materials and methods

2.1. Data

Daily maximum and minimum temperature and total precipitation from the European Centre for Medium-Range Weather Forecasts ERA5-Land reanalysis (Muñoz-Sabater et al., 2021) were used to identify CDHW events over the IP. ERA5-Land shares with ERA5 reanalysis (Hersbach et al., 2020) most of the parameterizations, which guarantee the use of the state-of-the-art land surface modelling, but has the advantage of improved horizontal resolution up to ~10 km. According to Muñoz-Sabater et al. (2021), this reanalysis exhibits an added value in describing the hydrological cycle by comparing against independent in situ observations, global models or satellite-based datasets.

In order to identify the origin of moisture and heat for the CDHW events, we used the atmospheric parcels trajectories from the global outputs from the Lagrangian FLEXible PARTicle (FLEXPART v10.3) dispersion model (Pisso et al., 2019). In this simulation, FLEXPART has been driven by the 3-hourly meteorological data from the ERA5 reanalysis at $0.5^{o} \times 0.5^{o}$ grid spacing and 137 vertical levels. The model homogeneously divided the atmosphere into 30 million air parcels with equal mass (Vázquez et al., 2024). Overall, FLEXPART represents the flowing atmosphere and enables the identification of moisture (e.g., Ramos et al., 2016; Gimeno et al., 2020; Pérez-Alarcón et al., 2022, 2023) and heat (e.g. Schumacher et al., 2020; Li et al., 2024) origins through parcel property changes along their trajectories when moved throughout the atmosphere by the 3D wind field.

2.2. Identification of drought conditions

Drought conditions have been widely identified using several indices, such as the Standardized Precipitation Index (McKee et al., 1993), Standardized Precipitation Evapotranspiration Index (Vicente-Serrano et al., 2010), Palmer Drought Severity Index (Palmer, 1965) or the self-calibrated Palmer Drought Severity Index (Wells et al., 2004). As they focus on different aspects of drought, they may produce different results (Mishra and Singh, 2010; Zhao et al., 2017; Hoffmann et al., 2020). These indices have been commonly used to detect dry periods at a monthly or longer scales, thus they are often not appropriate to monitor the daily condition of cumulative antecedent precipitation deficits (Park et al., 2022). As we are interested in CDHWs, we used the self-calibrating Effective Drought Index (scEDI; Park et al., 2022) to determine the onset and demise of drought conditions at the daily scale. The scEDI is a modification of the Effective Drought Index (Byun and

Wilhite, 1999) by using a rolling 30-year period (the preceding 30 years) to compute the effective precipitation normalcy. Further details on scEDI formulation can be found in Park et al. (2022).

By using the scEDI, a dry period starts when the scEDI value is lower than −0.5 and ends when the index is higher than 0.5, which leads to a more reliable assessment of drought frequency and duration (e.g., Kam et al., 2021). Furthermore, we defined the drought intensity by taking the minimum index value over the drought duration, in agreement with previous studies (e.g., Park et al., 2015; Kam et al., 2019). Based on the drought intensity, the events can be categorized into moderate ($-1.5 < \text{scEDI} \leq -0.5$), severe ($-2.5 < \text{scEDI} \leq -1.5$), and extreme ($\text{scEDI} \leq -2.5$).

2.3. Identification of heat waves

There are several definitions and metrics to describe and define heat waves (e.g., Russo et al., 2015; Sutanto et al., 2020; Becker et al., 2022; Díaz-Poso et al., 2023). In this study, the identification of heat waves consists of four steps. Firstly, we computed the daily maximum (minimum) temperature threshold for each grid point as the climatological 95th percentile of the daily maximum (minimum) air temperature on a 31-day window centred for the reference period 1991–2020. Secondly, we identified a warm event over a grid point if, at least during three consecutive days, the daily maximum and minimum temperatures

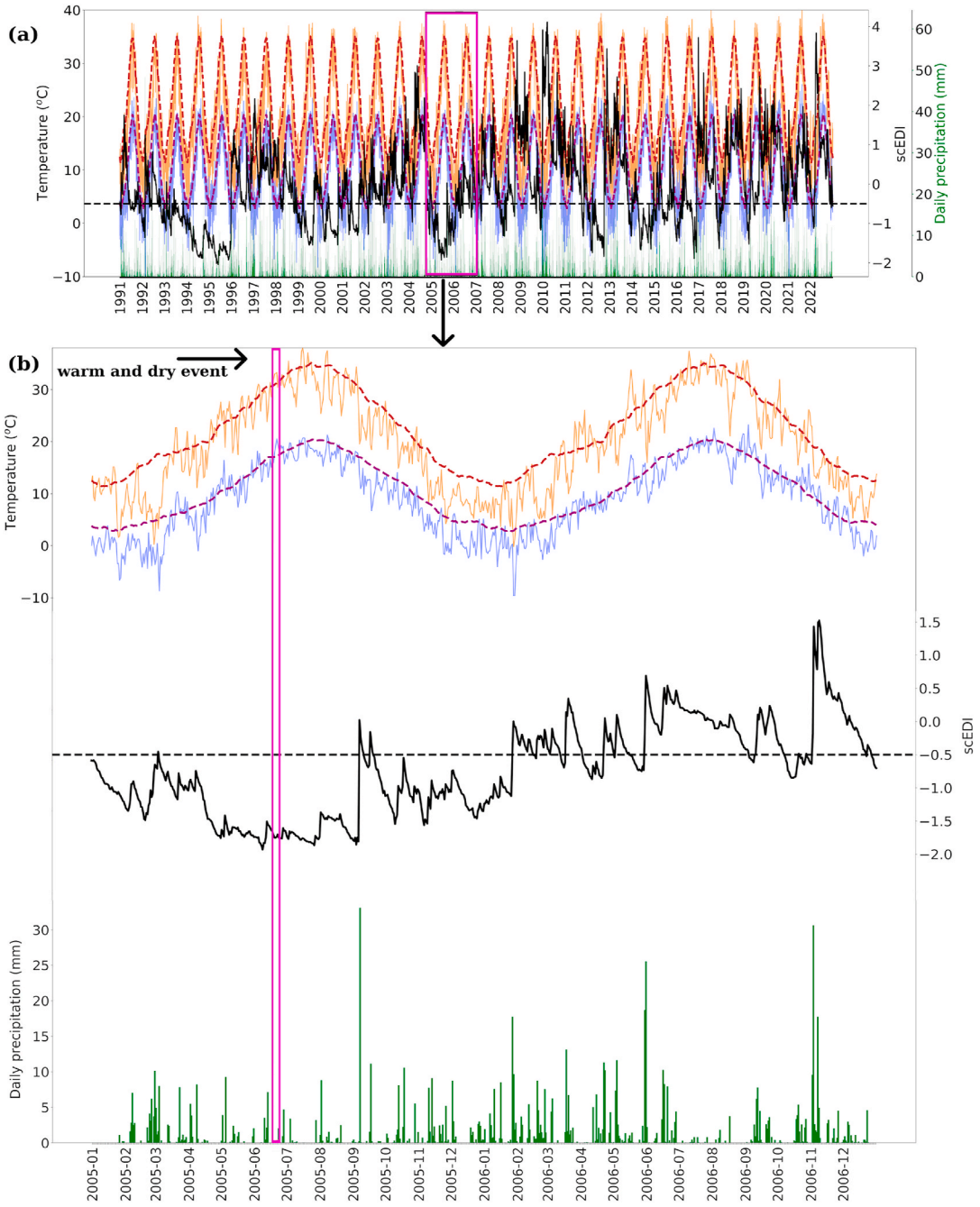

Fig. 1. **(a)** Time series of daily self-calibrating Effective Drought Index (scEDI, solid black line), daily maximum (solid orange line) and minimum (solid blue line) temperature and daily precipitation (green bars) extracted from the European Centre for Medium-Range Weather Forecasts ERA5-Land reanalysis from 1991 to 2022, for a single grid cell located in the southeastern IP. The dashed brown and purple lines show the daily 95th percentile of the maximum and minimum air temperature, while the dashed black line illustrates the threshold for the onset of a dry period. **(b)** Zoom of the pink box in **(a)** to illustrate the identification of a warm and dry event for the same grid cell from January 2005 to December 2006.

exceed the corresponding thresholds. Thirdly, a warm day in the study region is identified if at least 10% of the considered grid points show positive anomalies. It is worth noting that as heat waves are typically a synoptic-scale phenomenon (Stéfanon et al., 2014; Zschenderlein et al., 2019), we discarded small areas of high-temperature extremes by considering an affected area of at least 10%. Finally, three consecutive warm days must occur to have a heat wave.

To account for the intensity of a heat wave, Russo et al. (2015) proposed the percentile-based Heat Wave Magnitude Index daily (HWMId) as the sum of the magnitude of the consecutive days composing the event, with the daily magnitude calculated as follows:

$$HWMId(d) = \frac{T_d - T_{30y,P25}}{T_{30y,P75} - T_{30y,P25}}, \text{if } T_d > T_{30y,P25}, \text{otherwise}, HWMId(d) = 0$$

where T_d is the maximum temperature of the day d and $T_{30y,P25}$ ($T_{30y,P75}$) represent the 25th (75th) percentile of that calendar day computed from all 31-day centred time series of maximum air temperature within the reference period 1991–2020.

2.4. Identification of compound drought and heat wave events

A CDHW event is defined as a concurrent heat wave and drought in terms of location and time. As an example, following the identification criteria of droughts and heat waves, Fig. 1a displays the time series of the daily maximum and minimum air temperature, daily precipitation and scEDI from 1991 to 2022 at a single random grid point located in the southeastern IP, and Fig. 1b illustrates an instance when a warm and dry event takes place in late June 2005 at that grid point. If such a pattern is observed in at least 10% of the grid points, it will be considered a CDHW event. It is also important to remark that as heat waves frequently occur in the summer season in the IP (Sánchez-Benítez et al., 2020), we focused on CDHWs within the extended summer (May to October). Furthermore, multiple heat waves may exist within the same drought period. Therefore, if this was the case, those events are considered as different CDHW events.

2.5. Lagrangian moisture and heat sources identification

To identify moisture sources, we backtracked up to 10 days the precipitating air parcels residing over the affected area (the target region) of each CDHW event in the IP. Air parcel trajectories were extracted from the global simulations of the Lagrangian FLEXPART model (Vázquez et al., 2024), as described above. Several authors (e.g., Numaguti, 1999; van der Ent and Tuinenburg, 2017; Gimeno et al., 2021) have noted that about 10 days is the mean water vapour residence time in the atmosphere from evaporation to precipitation. In addition, previous studies (e.g., Li et al., 2024; Pérez-Alarcón et al., 2024a) have used a trajectory length of 10 days to identify sensible heat sources during heat wave events. Precipitating parcels were identified following Fremme and Sodemann (2019) as those parcels in which the relative humidity was higher than 80% over the target region and the specific humidity (q) decreased more than 0.1 g/kg in the 6 h before arrival at the region of interest. Additionally, we did not apply any distinction for moisture uptake ($\Delta q > 0$) within and above the boundary layer. Moisture changes along the parcel trajectory can occur due to evaporation or precipitation. Thus, we proportionally discounted moisture losses in route to all previous moisture uptake to obtain an objective picture of the origin of moisture that finally arrived at the target region, in agreement with Sodemann et al. (2008). Further details on the Lagrangian moisture source diagnostic method can be found in Sodemann et al. (2008) and Fremme and Sodemann (2019).

To account for heat sources, we followed an analogous method for moisture sources, quantifying the overall changes in the dry static energy (DSE) along the parcel trajectory, as described by Schumacher et al. (2020). In line with Schumacher et al. (2020), only air parcels arriving at the target region in the atmospheric boundary layer (ABL) were followed backwards in time up to 10 days to determine the origin of advected heat in the atmosphere. Additionally, air parcels that remained below the maximum ABL height between two consecutive 6-hourly periods during DSE uptakes were considered, and only 6-hourly changes in DSE >1 kJ/kg (corresponding to a potential temperature increase of 1 K) were diagnosed as a sensible heat uptake. Similarly to the moisture sources diagnostic, heat uptakes were corrected by linearly discounting cooling in route to all previous heat uptakes. Further details on the Lagrangian heat sources diagnostic approach can be found in Schumacher et al. (2020).

To obtain the total moisture and heat uptake during the CDHW event, we aggregated (averaged) the daily transport of moisture (heat) from surrounding and remote source regions over the event length. Both Lagrangian approaches were coded in Python in the Lagrangian atmospheric moisture and heat tracking (LATTIN) tool (Pérez-Alarcón et al., 2024b). Furthermore, as noted above, the target region was defined as the affected area by the CDHW event. Therefore, we only applied the Lagrangian heat and moisture sources diagnostic to all events affecting an area higher than 50% of the IP, guaranteeing a good representation of the study region for the climatological analysis. Finally, to compute the climatological sources for each event, we performed the Lagrangian analysis for the 6-hourly event dates from 1991 to 2020. The moisture (heat) transport anomalies were then estimated as the difference between the total moisture (heat) uptake during the event and the corresponding climatological value.

3. Results and discussion

3.1. Overview of CDHW events in the Iberian Peninsula

A total of 116 CDHW events (~3.6 events/year, Supplementary Table S1) were detected in the IP in the extended summer (May–October) from 1991 to 2022, leading to 729 days (~22.7 days/year) under dry and hot conditions. On average, a single event affected the IP for approximately 6.3 days. Note that, by definition, a CDHW should last for at least 3 days. Additionally, by a simple inspection of the CDHW time series, we detected the highest number of CDHWs in 2009, with 10, followed by 2018, with 9. Meanwhile, the extended summer of 2022 achieved the highest number of dry and hot days, namely 88. However, some years (e.g., 1996, 1997, 2007, 2010, 2013 and 2019) appear without any CDHW event, which can be presumably related to the generally wet, cold and generally unsteady conditions over the region. A seasonal analysis also revealed that August recorded the highest number of events, with 29, and September the lowest, with 9. Previously, Sánchez-Benítez et al. (2020) detected a similar seasonal distribution for heat waves in the IP. Fig. 2 displays the spatial distribution of the annual frequency of CDHWs in the IP, revealing the highest number of events (2.4–3.2 events/year) in the central-eastern IP region.

After filtering the events that affected more than 50% of IP, we retained the top 20 CDHWs, which occurred in 10 singular years within the 32-year study period. The highest number (4 events) was recorded in 2012, followed by 2015 and 2022, with 3 events. Again, 2022 registered the highest number of days under extreme dry and hot conditions, with 46 days, while the average duration of each top 20 CDHW was 10.35 days. Table 1 summarizes the main characteristics of these events. Note that the event ranked first (June 17, 2005, duration: 12 days) affected approximately 87.2% of the IP, while the ranked eighteenth (July 9, 2022, duration 18 days) registered the highest maximum and mean temperature and HWMI of all, although only extended for 51.3% of the area of the study region.

Fig. 3 shows the affected area, maximum temperature anomalies and drought intensity for the events in the top five, while Supplementary Figs. S1 and S2 illustrate these metrics for the remaining events. Overall, the air temperature anomalies during these CDHWs varied from 2 to 8 °C, and droughts can be categorized as moderate and severe, except for

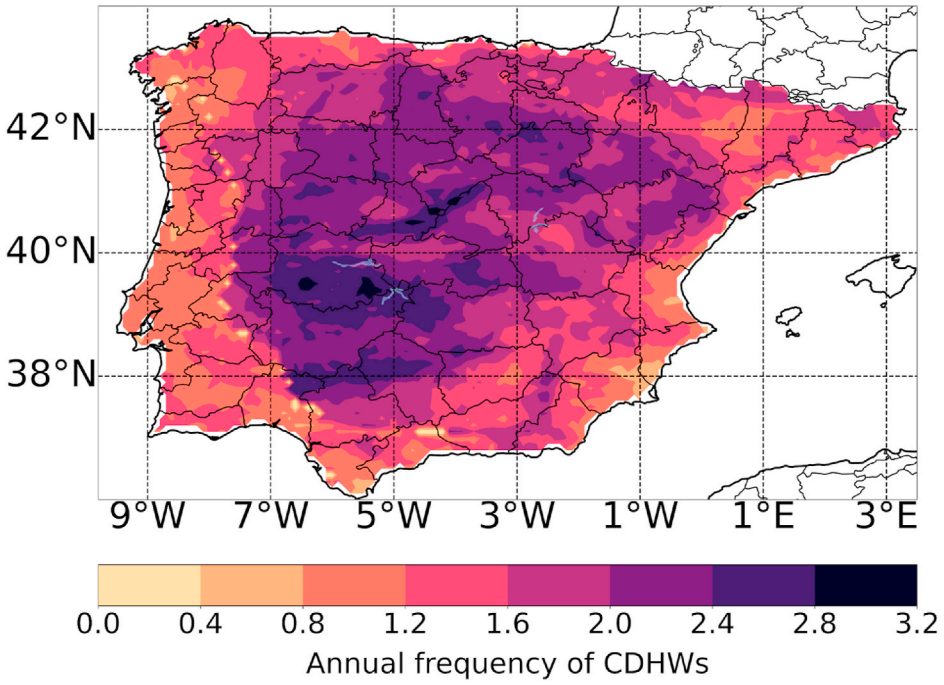

Fig. 2. Annual frequency of compound drought and heat wave events in the Iberian Peninsula from 1991 to 2022.

Table 1
Main characteristics of the 20 CDHWs that affected more than 50% of the IP in the extended summer (May–October) from 1991 to 2022. HWMI: Heat wave magnitude index, DI: Drought intensity. Tmax and Tmean represent the highest maximum temperature and the average maximum temperature recorded during the event, respectively.

Rank	Start	Duration (days)	Tmax (°C)	Tmean (°C)	HWMI	DI	Area (%)
1	June 17, 2005	12	40.5	37.5	51.2	−3.1	87.2
2	June 24, 2012	7	43.3	41.8	31.8	−2.2	75.7
3	August 17, 2012	13	42.2	39.3	54.1	−2.6	68.7
4	October 26, 2009	7	30.8	29.7	24.3	−2.2	63.7
5	September 15, 1991	10	38.5	35.7	37.6	−1.7	63.3
6	May 10, 1991	5	37.7	34.6	25.4	−1.6	60.4
7	May 1, 1995	9	32.1	29.7	58.9	−2.4	60.4
8	September 16, 2012	8	35.2	33.6	31.2	−3.0	59.1
9	June 8, 2017	18	42.3	39.4	70.5	−2.1	58.7
10	July 12, 2015	12	41.5	40.0	48.9	−1.9	58.6
11	June 9, 2022	12	42.4	40.7	57.9	−1.8	57.1
12	May 26, 2006	5	36.9	34.8	25.4	−2.6	55.8
13	September 1, 2006	11	41.1	37.4	50.1	−2.6	55.3
14	July 29, 2022	16	41.6	39.6	64.1	−2.7	53.5
15	October 25, 1995	4	31.8	29.8	15.0	−2.1	52.0
16	June 26, 2015	14	43.5	41.0	59.2	−1.4	51.4
17	May 9, 2012	10	37.8	35.5	35.8	−2.3	51.4
18	July 9, 2022	18	44.2	42.1	83.8	−2.0	51.3
19	May 22, 2017	7	35.9	34.3	53.8	−2.7	50.8
20	June 1, 2015	9	37.4	35.6	31.3	−2.0	50.3

the event ranked first, third and eight (Fig. 3 and S2), which exhibited extreme drought conditions in most of the affected area. Interestingly, events in October and May generally recorded relatively low maximum air temperatures (Table 1). However, they registered high maximum temperature anomalies, probably favoured by the severe dry conditions. As previously noted by Stéfanon et al. (2014), the lack of moisture in the lower atmosphere and soils (Supplementary Fig. S3) during drought episodes leads to a positive feedback favouring the dry and hot conditions.

3.2. Climatological heat and moisture sources

By taking the shaded areas in Fig. S1 as target regions for the Lagrangian analysis of each CDHW event, we computed changes in specific humidity and DSE using the 10-day backward trajectories from the global outputs of the FLEXPART model of all precipitating air parcels over the target region for moisture sources and all parcels arriving within the ABL at the target region for heat sources, respectively.

Several studies (e.g., Gimeno et al., 2010; Rios-Entenza and Miguez-Macho, 2014; Liu et al., 2022; Alvarez-Socorro et al., 2023) have identified the origin of precipitation over the IP. The most important moisture source regions are the subtropical North Atlantic corridor, the IP itself throughout the recycling process and the Mediterranean Sea. On this basis, Fig. 4 displays the climatological accumulated moisture uptake from the Lagrangian backtracking analysis for the dates of the CDHW events listed in Table 1 and supports these previous results. Note that the climatological moisture contribution to the target regions defined by the affected area of the CDHW events generally decreases as

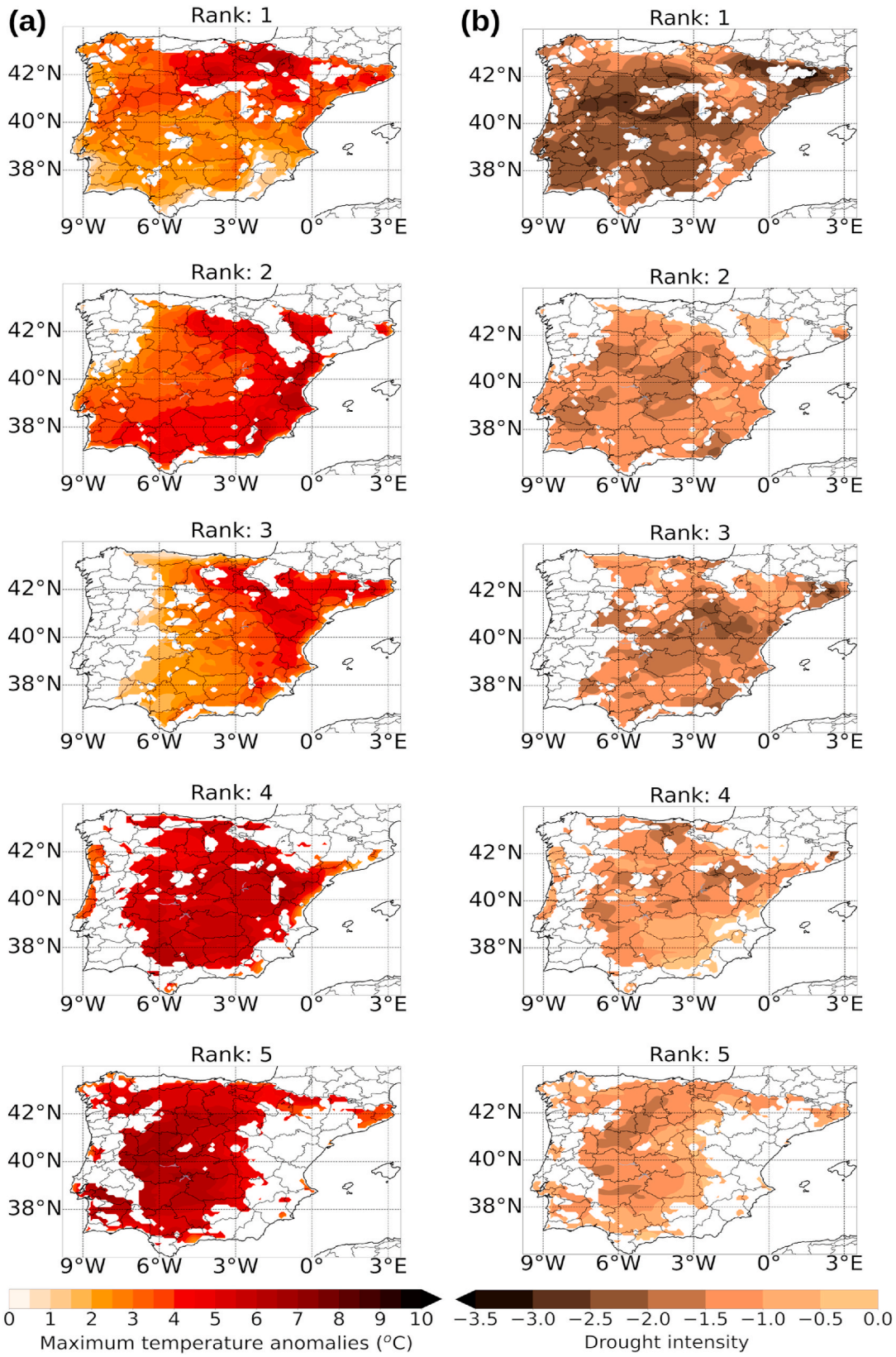

Fig. 3. **(a)** Spatial distribution of the maximum air temperature anomalies and **(b)** drought intensity during the top 5 compound drought and heat wave events in Iberian Peninsula ranked according to the affected area (see Table 1) in the extended summer (May–October) from 1991 to 2022. The maximum temperature anomalies were computed using the climatological maximum temperature for the same dates of each event in the reference period 1991–2020.

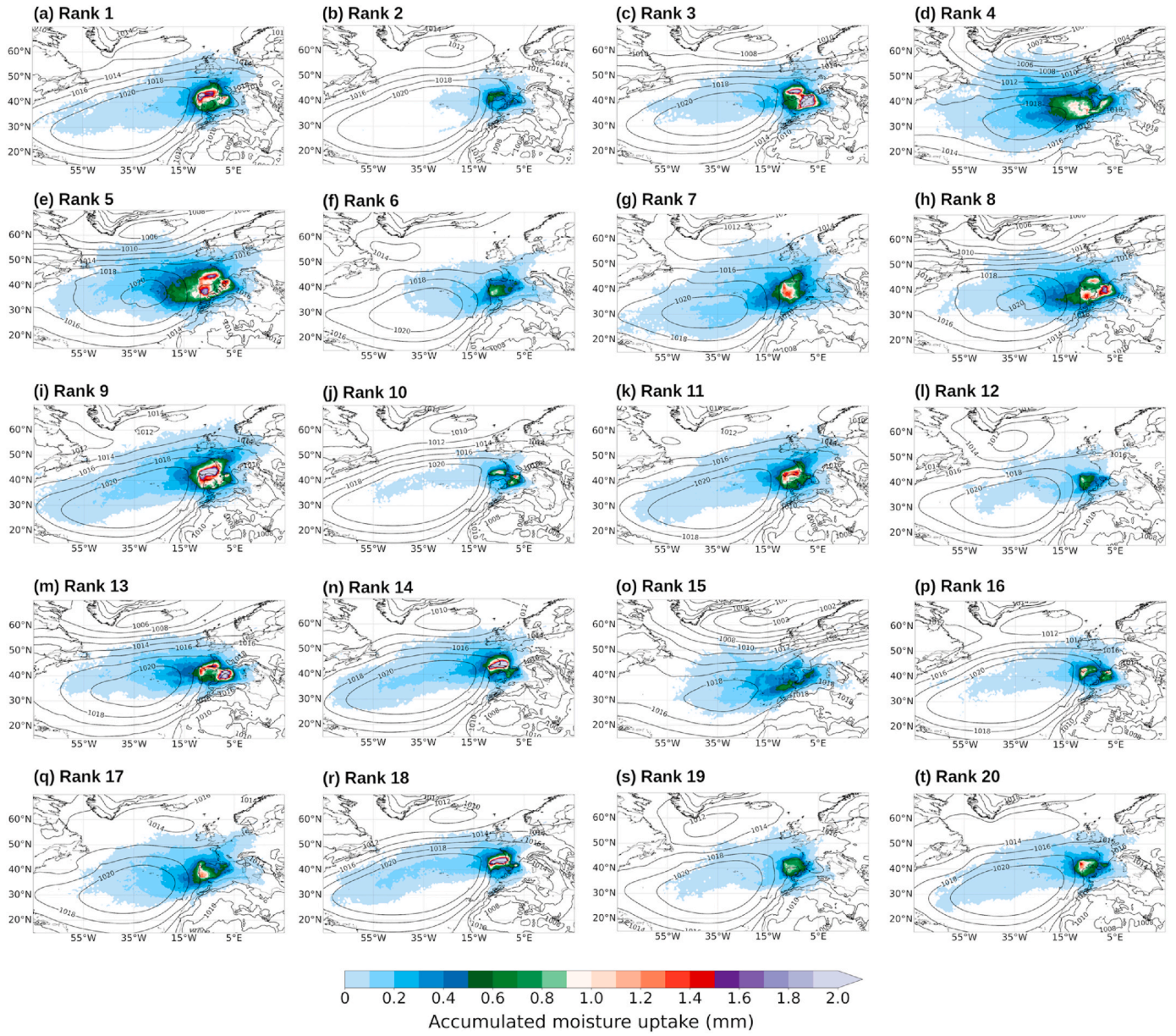

Fig. 4. Climatological accumulated moisture uptake (shaded) for the same dates (month and day) of the CDHW events listed on Table 1 from 1991 to 2020. Contour lines denote the climatological mean sea level pressure during each event.

its distance to them increases. Fig. 4 also shows that the subtropical high controls the atmospheric circulation over the IP, suggesting that the descending air associated effectively leads to suppression of cloudiness and thus to a noticeable decrease in the summertime precipitation by reducing the moisture contribution from the Atlantic Ocean, as previously found by Liu et al. (2022). Likewise, the moisture arriving from the Mediterranean Sea is small or negligible in most of the cases. These mechanisms highlight the recycling process, and consequently local convective events, as a key mechanism for precipitation summer, as revealed by the climatological moisture source patterns in Fig. 4.

Similarly, climatological heat sources cover the entire IP, further extending into the northern Atlantic Ocean and encompassing some parts of northern Africa and western Europe (Fig. 5), although the heat contribution from the later sources is noticeably weak. Santos et al. (2015) applied the Lagrangian analysis tool LAGRANTO (Sprenger and Wernli, 2015) and detected that air parcels crossing the northern Atlantic Ocean contribute to extremely warm summer temperatures over the IP. However, while these authors accounted for all temperature changes along the parcel's trajectories, we only accounted for those changes within the ABL. It is well-known that subsidence increases air mass temperature through adiabatic compression heating, as also shown for the IP (Bieli et al., 2015; Santos et al., 2015; Zschenderlein et al., 2019). Therefore, parcels travelling above the ABL and rapidly descending over the target region play a crucial role in extreme temperature events (Santos et al., 2015). This relationship is evident by counting the number of air parcels residing over the affected area during each CDHWs. While the total number of parcels over the target region ranged from 25 000 to 30 000 at each 6-hourly time step, approximately ~13% (Fig. S4) of them were within the ABL and used for the Lagrangian sensible heat sources identification.

Overall, the westerly and northwesterly flow from the northern Atlantic basin associated with the northern branch of the high-pressure system leads to advection of the warmed air parcels to the target regions. Furthermore, the climatological heat source patterns shown in Fig. 5 confirms the local-to-regional origin of sensible heat flux for IP, in contrast to the remote origin of warm air masses for central and northern

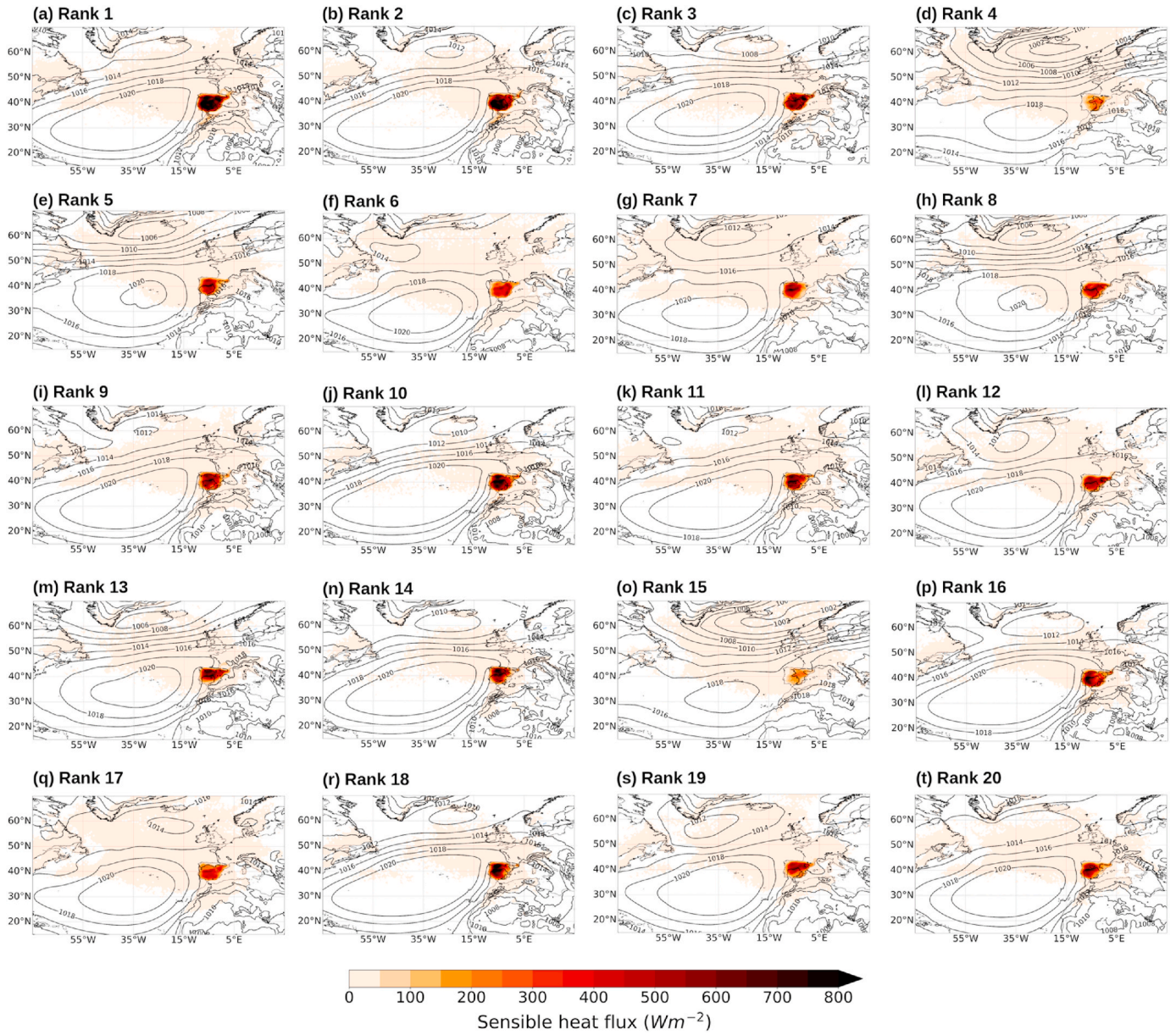

Fig. 5. Climatological daily sensible heat flux during the same dates (month and day) of the CDHW events listed on Table 1 from 1991 to 2020. Contour lines denote the climatological mean sea level pressure during each event.

Europe (Santos et al., 2015; Sousa et al., 2019; Rousi et al., 2023).

3.3. Moisture and sensible heat flux anomalies during CDHWs

Dry and heat conditions are exacerbated during CDHWs. Figs. 6 and 7 illustrate the anomalies in terms of accumulated moisture uptake and sensible heat flux for the top 20 cases, also depicting the mean sea level pressure (MSLP) anomalies. A common pattern among all the events is positive MSLP anomalies influencing the IP region, resembling the role of subsidence in favouring extreme warm temperatures. Previously, Sánchez-Benítez et al. (2020) addressed that IP heat waves generally occur during weather regimes associated with ridge conditions in western Europe.

The predominantly high pressures over the IP, either in the form of an atmospheric blocking or a ridge, lead to a noticeable drop in the summertime precipitation (e.g., Santos et al., 2009; Sousa et al., 2017; Liu et al., 2022), decreasing more drastically during CDHWs. Negative accumulated moisture uptake anomalies are mostly observed among all of the moisture sources during each event. Note that regions under drought conditions (see shaded areas in Fig. S1) tend to provide less moisture (Fig. S3), reducing the moisture recycling over the IP, which is often a moisture source for precipitation in summer. It is important to note that some footprints of positive anomalies are detected over northwestern Africa and the eastern North Atlantic, especially for events ranked seventh and fifteenth, respectively. Interestingly, all cases showing above-average accumulated moisture supplied from some source regions occurred in May or October, which can be linked to changes in the atmospheric circulation patterns during these months.

In contrast to the moisture contributions, the sensible heat flux anomalies shown in Fig. 7 reveal negative anomalies over the northern IP and Atlantic Ocean during most of the CDWHs and positive ones extending from southern IP to northern Africa. These patterns confirm that the heat imported from northern Africa plays a crucial role in IP heat waves, in agreement with Sousa et al. (2019). Despite the observed negative anomalies, the heat waves were favoured by the reduction in evaporative cooling due to the concurrent drought conditions and the

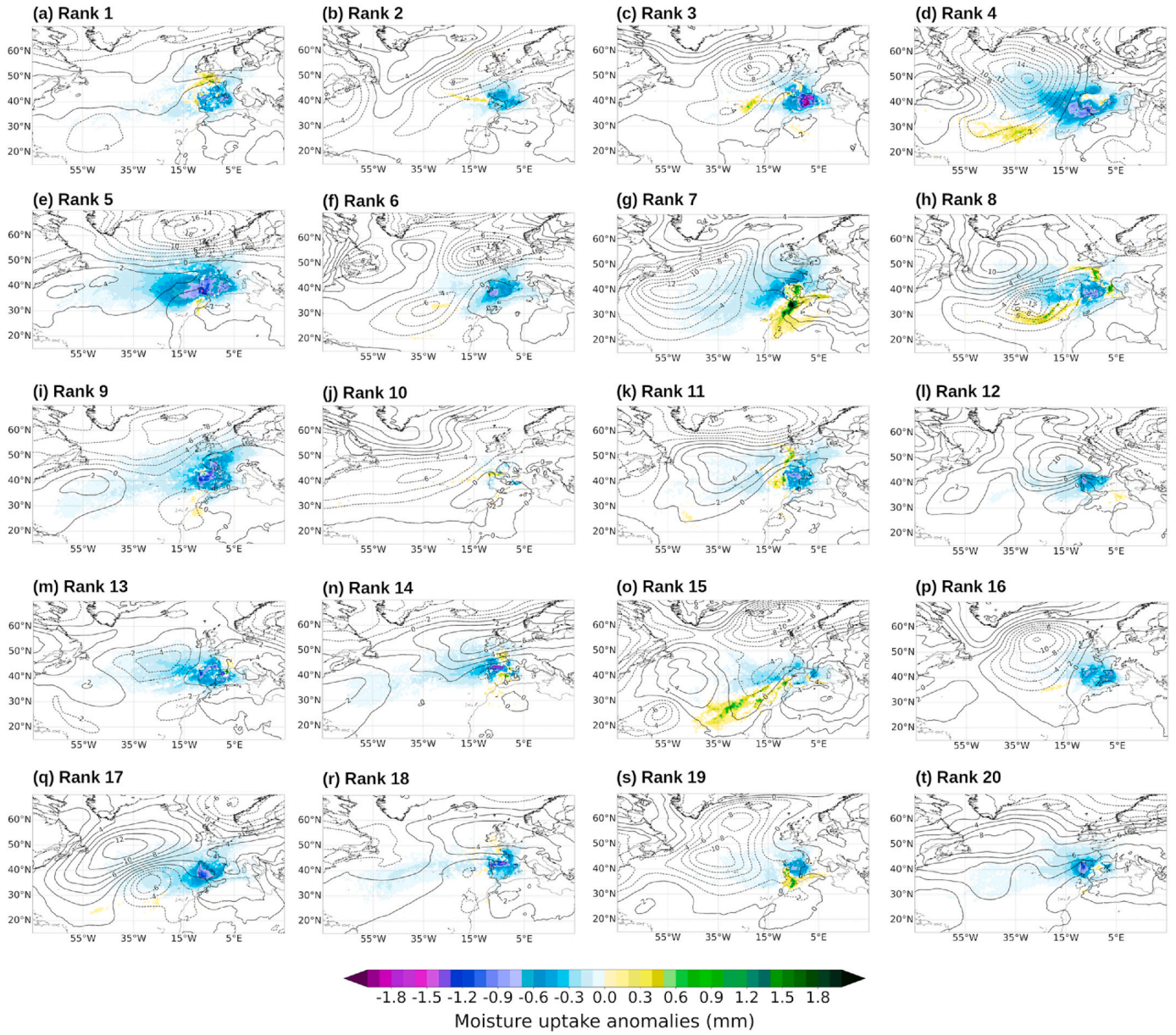

Fig. 6. Anomalies in the accumulated moisture uptake during the CDHW events listed on Table 1. The anomalies were computed as the difference between the accumulated moisture uptake during the event and the climatological accumulated moisture uptake for the same dates of the event. Shaded regions mark anomalies larger than one standard deviation. Solid (dashed) contour lines denote positive (negative) anomalies in the mean sea level pressure.

consequently decrease in soil moisture (Fig. S3), intensifying the event through land-atmosphere feedback, in agreement with e.g. Hauser et al. (2017). This mechanism contributed to the intensification of the Russian heat wave in 2010 (e.g., Barriopedro et al., 2011; Trenberth and Fasullo, 2012). In addition, according to Miralles et al. (2014), the soil moisture deficit leads to the entrainment of warm air during the day and the formation of a warm residual layer above the ABL at night retaining heat over night. This heat can reenter into the mixed layer the next day. Note that this heat stored above the ABL is not accounted for during the Lagrangian tracking analysis, as we are interested in identifying sensible heat sources. Therefore, this finding also stresses the importance of the subsidence in the increasing temperature of air parcels, thereby contributing to the development of heat waves over the IP. Indeed, the soil-atmosphere feedback thought the diabatic heating effect induced by the drought conditions may play a role in maintaining the high-pressure conditions, in agreement with Rousi et al. (2023) and Zhou et al. (2024).

Despite the areas with negative anomalies in the sensible heat flux, we can expect negative (positive) anomalies in the total contribution from moisture (heat) sources. This hypothesis is confirmed in Fig. 8 by computing the overall changes in the accumulated moisture uptake and average daily sensible heat flux during each CDHW. In line with the results in Fig. 6, Fig. 8a highlights that the total accumulated precipitating moisture is reduced by 15%–80% when compared with its climatological value. This means that the contribution to precipitation is disproportionately low during CDHW events. The sensible heat contributions show an increase for most of the events, being, on average, 5%–75% higher than the climatological heat contribution and reaching 125% above normal for the event ranked twentieth (Fig. 8b). We considered that these overall sensible heat flux positive anomalies enhanced the diabatic heating and consequently the hot conditions, which is aligned with previous studies on extreme heat waves (e.g., Hong et al., 2022; Liu et al., 2024; Zhou et al., 2019, 2024). However, it is worth noting that events ranked fourth (R04; ~34%), sixth (R06; ~15%) and fifteenth (R15; ~35%) achieved an overall reduction in the

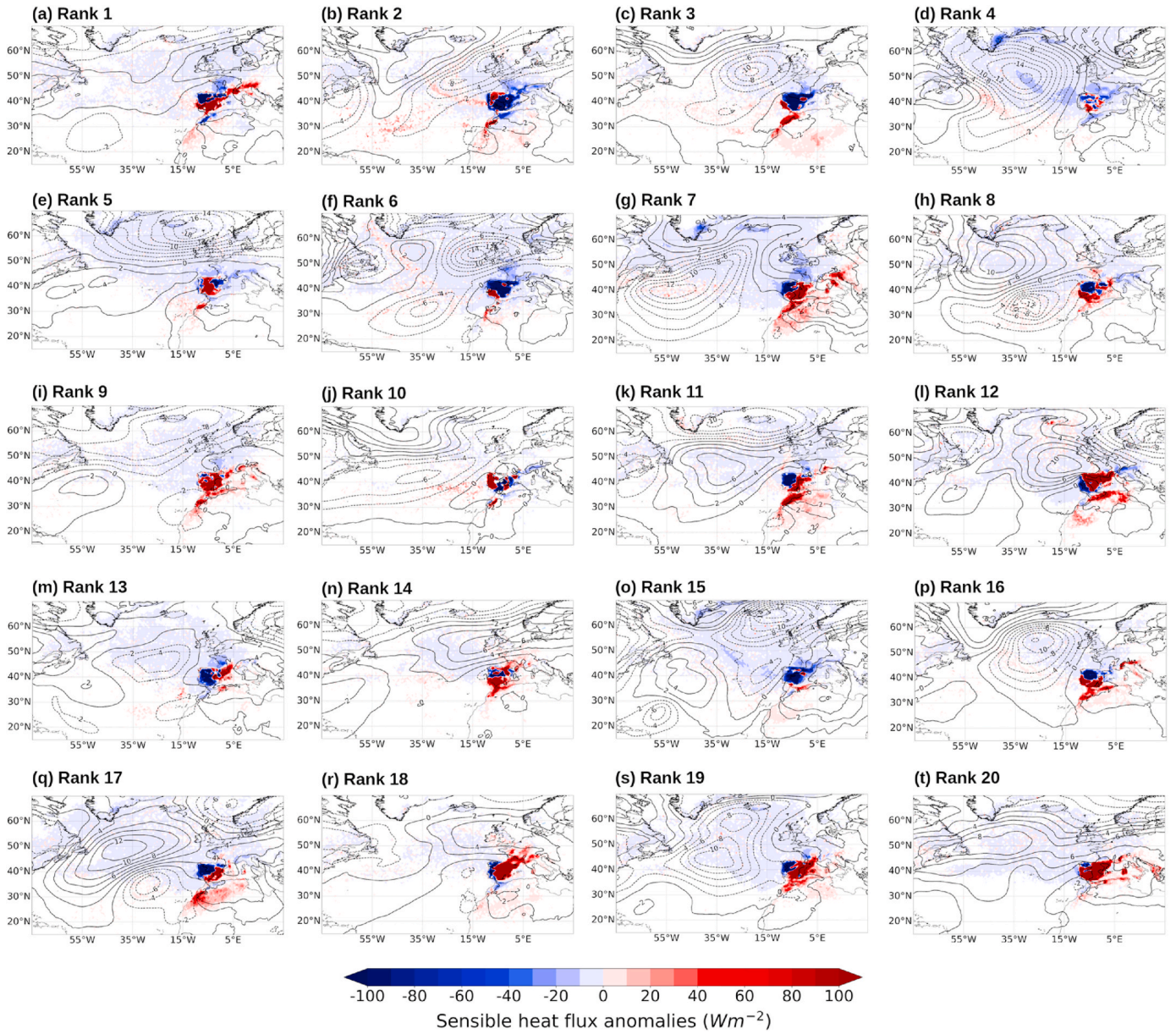

Fig. 7. As Fig. 6 but for the daily sensible heat flux.

total sensible heat contributions. These below-average events occurred in May (event ranked sixth) and October (events ranked fourth and fifteenth), suggesting a different role of atmospheric circulation during transitioning months. In addition, there is currently no agreement on the relative contributions of physical processes (i.e., temperature advection, adiabatic warming due to subsidence, and diabatic heating from surface sensible heat fluxes) that lead to the development of a heat wave (e.g., Garfinkel and Harnik, 2017; Miralles et al., 2019; Wehrli et al., 2022). Consequently, the negative sensible heat flux anomalies observed in these CDHWs (R04, R06, R15) also suggest that these events were primarily driven by adiabatic warming rather than temperature advection or sensible heating. Indeed, Santos et al. (2015) highlighted the role of adiabatic warming in driving heat waves in the IP.

4. Final remarks and conclusions

In this study we have examined CDHWs over the IP during the extended summer (May–October) from 1991 to 2022 by applying a novel Lagrangian moisture and sensible heat tracking framework. The analysis of the life-cycle of the top 20 events ranked by the affected area revealed that they are relatively long-lived, achieving a mean duration of ~10.35 days, with 2022 recording a total of 46 days under dry and hot conditions. From a climatological viewpoint, CDWHs over the IP are generally associated with the influence of blocking situations characterized by the presence at the surface of anticyclones and/or atmospheric ridges. Fig. 9 summarizes climatological patterns of moisture and sensible heat sources and the corresponding moisture and heat contribution anomalies among all of the 20 events (listed on Table 1). The moisture and heat tracking analysis revealed a climatological local-to-regional origin of moisture (Fig. 9a) and heat (Fig. 9b) during the event's dates, being the IP itself the main moisture and heat source.

The spatial distribution of the accumulated moisture uptake anomalies (Fig. 9c) shows below-average moisture support during the CDHW events, influenced by the persistent subsidence associated with the high pressures over the IP. Additionally, negative anomalies were observed in the heat contribution from the northern Atlantic Ocean and northwestern IP and positive anomalies in the remaining IP region further extended to northern Africa (Fig. 9d). We hypothesize that the

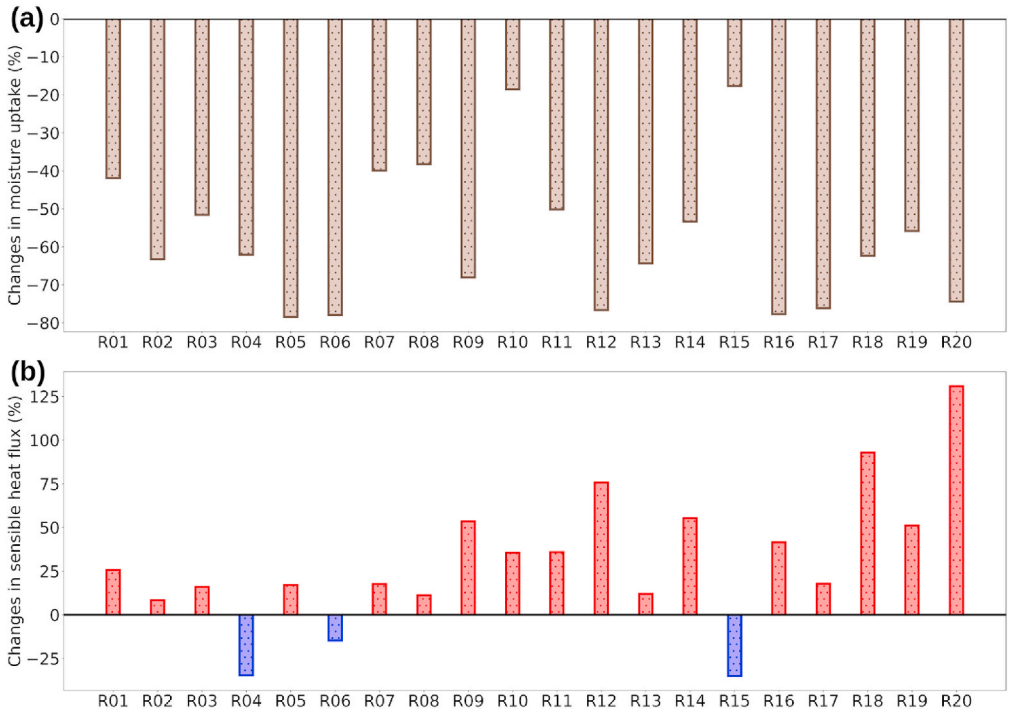

Fig. 8. Changes in the total **(a)** accumulated moisture uptake and **(b)** daily sensible heat flux during each CDHW event with respect to the climatological value. Hatches indicate statistically significant ($p < 0.05$) changes in moisture uptake and sensible heat fluxes.

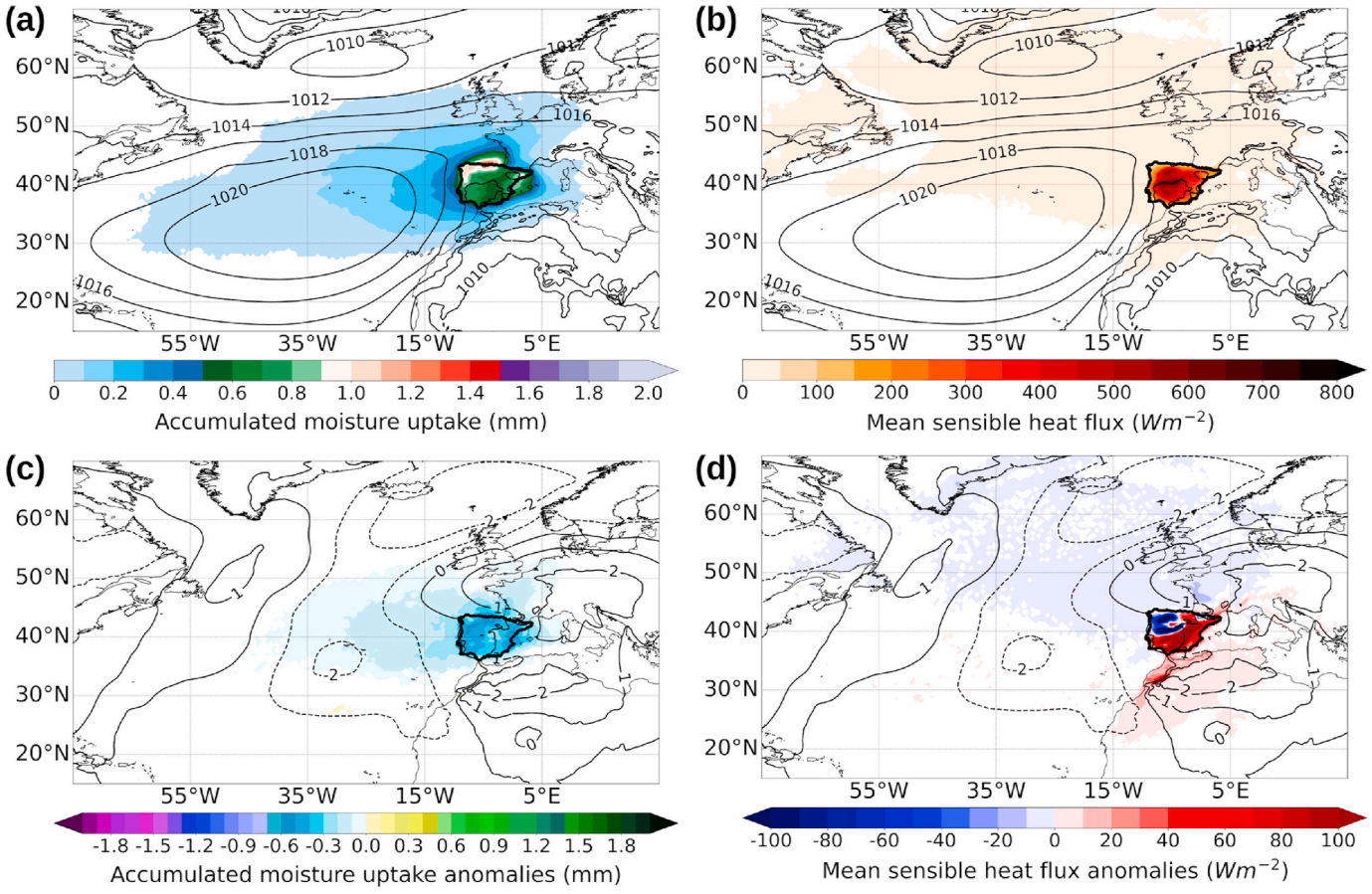

Fig. 9. Mean climatological **(a)** accumulated moisture uptake and **(b)** daily sensible heat flux during the CDHW events listed in Table 1. Contour lines represent climatological mean sea level pressure. Panels **(c)** and **(d)** show mean anomalies for accumulated moisture uptake and sensible heat flux, respectively. Solid (dashed) contour lines denote positive (negative) anomalies in the mean sea level pressure. Bold black line denotes the IP region.

concurrent dry conditions are associated with low soil moisture (Fig. S3), and thus a reduction of the evaporative cooling, which may contribute to the development and persistence of the event through land-atmosphere feedback (Barriopedro et al., 2023). Overall, during CDHWs in the IP, the moisture contribution decreases by about 56%, and the sensible heat support increases by approximately 35%.

Building on previous works mostly focused on atmospheric circulation associated with dry and hot conditions in the IP and/or Western Europe (e.g., Santos et al., 2015; Sánchez-Benítez et al., 2020; Liu et al., 2022; Díaz-Poso et al., 2023; Rousi et al., 2023), this study emphasizes the local-to-regional origins of moisture and sensible heat anomalies and their amplification through land-atmosphere feedbacks during CDHW events. While previous studies acknowledged the role of subsidence and soil moisture deficits in CDHW events (e.g., Mukherjee et al., 2020; Kautz et al., 2022; Hao et al., 2022; Barriopedro et al., 2023; Rousi et al., 2023), this work integrates these dynamics with sensible heat and moisture source contributions, offering a more comprehensive understanding of CDHW mechanisms. In particular, our results provided evidence that the below-average moisture and above-average sensible heat source contributions are linked and amplified by the predominately high-pressure conditions and soil moisture deficits observed during such extremes. Furthermore, the top 20 CDHWs could serve as case studies to enhance our understanding of the underlying mechanisms of these compound climate extremes. This work also highlights the added value of the novel Lagrangian atmospheric moisture and heat tracking framework for studying CDHWs, which could be a powerful tool to enhance regional risk assessments and to investigate future changes in these extreme events under global warming. However, it is worth noting that the Lagrangian model and moisture and heat tracking methods have some uncertainties and limitations, such as the neglecting the mixing of air parcels, the evaporation of precipitating hydrometeors, numerical diffusion and numerical errors linked to the trajectory calculation. Furthermore, the ABL is assumed to be well mixed, which means that dry static energy increases reflect surface sensible heat fluxes, and the moisture and heat tracking framework does not provide a comprehensive causal relationship between the underlying mechanisms and CDHW events. Therefore, future research should be performed to help in understanding the complex physical processes that contribute to CDHWs in the context of global warming.

CRediT authorship contribution statement

Albenis Pérez-Alarcón: Writing – review & editing, Writing – original draft, Visualization, Validation, Software, Methodology, Investigation, Formal analysis, Data curation, Conceptualization. **Marta Vázquez:** Writing – review & editing, Software, Methodology, Investigation, Formal analysis, Conceptualization. **Alexandre M. Ramos:** Writing – review & editing, Validation, Supervision, Methodology, Investigation, Conceptualization. **Raquel Nieto:** Writing – review & editing, Validation, Supervision, Methodology, Investigation, Funding acquisition. **Joaquim G. Pinto:** Writing – review & editing, Validation, Supervision, Methodology, Investigation, Funding acquisition, Conceptualization. **Luis Gimeno:** Writing – review & editing, Validation, Supervision, Methodology, Investigation, Funding acquisition, Conceptualization.

Funding

This work is supported by Xunta de Galicia (Consellería de Cultura, Educación, Formación Profesional e Universidades) under the Postdoctoral grants No. ED481B-2023/016 and ED481D 2022/020, by the SETESTRELO project under grant no. PID2021-122314OB-I00, funded by the Ministerio de Ciencia, Innovación y Universidades, Spain (MICIU/AEI/10.13039/501100011033) and by the ESMORGA project (grant no. TED2021-129152B-C43) funded by MCIN/AEI/10.13039/501100011033 and the European Union NextGenerationEU/PRTR. Partial support was also obtained from the Xunta de Galicia under the Project ED431C 2021/44 (Programa de Consolidación e Estructuración de Unidades de Investigación Competitivas (Grupos de Referencia Competitiva) and Consellería de Cultura, Educación e Universidade) and by the European Union 'ERDF A way of making Europe'. AMR is funded by the Helmholtz Association program "Changing Earth" at KIT. JGP is funded by the AXA Research Fund.

Declaration of competing interest

The authors declare that they have no known competing financial interests or personal relationships that could have appeared to influence the work reported in this paper.

Acknowledgments

A.P-A. and M.V thank the support from the Xunta de Galicia (Consellería de Cultura, Educación, Formación Profesional e Universidades) under the Postdoctoral grants No. ED481B-2023/016 and ED481D-2022/020, respectively. A.P-A. also thanks the support by the ESMORGA project (grant no. TED2021-129152B-C43) funded by MCIN/AEI/10.13039/501100011033 and the European Union NextGenerationEU/PRTR during the research stay at KIT. EPhysLab members are supported by the SETESTRELO project (grant no. PID2021-122314OB-I00) funded by the Ministerio de Ciencia, Innovación y Universidades, Spain (MICIU/AEI/10.13039/501100011033), Xunta de Galicia under the Project ED431C2021/44 (Programa de Consolidación e Estructuración de Unidades de Investigación Competitivas (Grupos de Referencia Competitiva) and Consellería de Cultura, Educación e Universidade), and by the European Union 'ERDF A way of making Europe'. AMR and JGP thank the support from the Helmholtz Association program "Changing Earth" at KIT and the AXA Research Fund, respectively. This work has also been possible thanks to the computing resources and technical support provided by CESGA (Centro de Supercomputación de Galicia) and RES (Red Española de Supercomputación).

Appendix A. Supplementary data

Supplementary data to this article can be found online at https://doi.org/10.1016/j.wace.2025.100756.

Data availability

The European Centre for Medium-Range Weather Forecasts ERA5-Land and ERA5 reanalysis can be freely downloaded through the C3S Climate Data Store at https://doi.org/10.24381/cds.e2161bac and https://doi.org/10.24381/cds.143582cf, respectively. The FLEXPART outputs can be obtained upon request from https://doi.org/10.5281/zenodo.13682647. The Python implementation for computing the self-calibrating Effective Drought Index can be obtained from Park et al. (2022), while the Lagrangian atmospheric moisture and heat tracking (LATTIN) tool is accessible through its GitHub repository at https://github.com/apalarcon/LATTIN.

References

Algarra, I., Nieto, R., Ramos, A.M., Eiras-Barca, J., Trigo, R.M., Gimeno, L., 2020. Significant increase of global anomalous moisture uptake feeding landfalling Atmospheric Rivers. Nat. Commun. 11 (1), 5082. https://doi.org/10.1038/s41467-020-18876-w.

Alvarez, I., Pereira, H., Lorenzo, M.N., Picado, A., Sousa, M.C., Taboada, J.J., Dias, J.M., 2024. Drought projections for the NW Iberian Peninsula under climate change. Clim. Dyn. 1–17. https://doi.org/10.1007/s00382-023-07084-z.

Alvarez-Socorro, G., Fernández-Alvarez, J.C., Nieto, R., 2023. Moisture source analysis of two case studies of major extreme precipitation events in summer in the Iberian Peninsula. Atmosphere 14 (8), 1213. https://doi.org/10.3390/atmos14081213.

Barichivich, J., Osborn, T., Harris, I., van der Schrier, G., Jones, P., 2019. Drought: monitoring global drought using the self-calibrating palmer drought severity index.

Bull. Am. Meteorol. Soc. 100 (9), S39–S40. https://doi.org/10.1175/2019BAMSStateoftheClimate.1.
Barriopedro, D., Fischer, E.M., Luterbacher, J., Trigo, R.M., García-Herrera, R., 2011. The hot summer of 2010: redrawing the temperature record map of Europe. Science 332 (6026), 220–224. https://doi.org/10.1126/science.1201224.
Barriopedro, D., García-Herrera, R., Ordóñez, C., Miralles, D.G., Salcedo-Sanz, S., 2023. Heat waves: physical understanding and scientific challenges. Rev. Geophys. 61 (2), e2022RG000780. https://doi.org/10.1029/2022RG000780.
Becker, F.N., Fink, A.H., Bissolli, P., Pinto, J.G., 2022. Towards a more comprehensive assessment of the intensity of historical European heat waves (1979–2019). Atmos. Sci. Lett. 23 (11), e1120. https://doi.org/10.1002/asl.1120.
Berg, A., Lintner, B.R., Findell, K., Malyshev, S., Loikith, P., Gentine, P., 2014. Impact of soil moisture–atmosphere interactions on surface temperature distribution. J. Clim. 27 (21), 7976–7993. https://doi.org/10.1175/JCLI-D-13-00591.1.
Bieli, M., Pfahl, S., Wernli, H., 2015. A Lagrangian investigation of hot and cold temperature extremes in Europe. Q. J. R. Meteorol. Soc. 141 (686), 98–108. https://doi.org/10.1002/qj.2339.
Brás, T.A., Seixas, J., Carvalhais, N., Jägermeyr, J., 2021. Severity of drought and heatwave crop losses tripled over the last five decades in Europe. Environ. Res. Lett. 16 (6), 065012. https://doi.org/10.1088/1748-9326/abf004.
Byun, H.R., Wilhite, D., 1999. Objective quantification of drought severity and duration. J. Clim. 12 (9), 2747–2756. https://doi.org/10.1175/1520-0442(1999)012<2747:OQODSA>2.0.CO;2.
Carvalho, D., Cardoso Pereira, S., Rocha, A., 2021. Future surface temperature changes for the Iberian Peninsula according to EURO-CORDEX climate projections. Clim. Dyn. 56, 123–138. https://doi.org/10.1007/s00382-020-05472-3.
Chen, L., Chen, X., Cheng, L., Zhou, P., Liu, Z., 2019. Compound hot droughts over China: identification, risk patterns and variations. Atmos. Res. 227, 210–219. https://doi.org/10.1016/j.atmosres.2019.05.009.
Christensen, J.H., Christensen, O.B., 2003. Severe summertime flooding in Europe. Nature 421 (6925), 805–806. https://doi.org/10.1038/421805a.
Di Luca, A., de Elía, R., Bador, M., Argüeso, D., 2020. Contribution of mean climate to hot temperature extremes for present and future climates. Weather Clim. Extrem. 28, 100255. https://doi.org/10.1016/j.wace.2020.100255.
Díaz-Poso, A., Lorenzo, N., Royé, D., 2023. Spatio-temporal evolution of heat waves severity and expansion across the Iberian Peninsula and Balearic islands. Environ. Res. 217, 114864. https://doi.org/10.1016/j.envres.2022.114864.
Fink, A.H., Brücher, T., Krüger, A., Leckebusch, G.C., Pinto, J.G., Ulbrich, U., 2004. The 2003 European summer heatwaves and drought-synoptic diagnosis and impacts. Weather 59 (8), 209–216. https://doi.org/10.1256/wea.73.04.
Fremme, A., Sodemann, H., 2019. The role of land and ocean evaporation on the variability of precipitation in the Yangtze River valley. Hydrol. Earth Syst. Sci. 23, 2525–2540. https://doi.org/10.5194/hess-23-2525-2019.
García-León, D., Casanueva, A., Standardi, G., Burgstall, A., Flouris, A.D., Nybo, L., 2021. Current and projected regional economic impacts of heatwaves in Europe. Nat. Commun. 12 (1), 5807. https://doi.org/10.1038/s41467-021-26050-z.
Garfinkel, C.I., Harnik, N., 2017. The non-Gaussianity and spatial asymmetry of temperature extremes relative to the storm track: the role of horizontal advection. J. Clim. 30 (2), 445–464. https://doi.org/10.1175/JCLI-D-15-0806.1.
Gimeno, L., Vázquez, M., Eiras-Barca, J., Sorí, R., Stojanovic, M., Algarra, I., et al., 2020. Recent progress on the sources of continental precipitation as revealed by moisture transport analysis. Earth Sci. Rev. 201, 103070. https://doi.org/10.1016/j.earscirev.2019.103070.
Gimeno, L., Eiras-Barca, J., Durán-Quesada, A.M., Dominguez, F., van der Ent, R., Sodemann, H., et al., 2021. The residence time of water vapour in the atmosphere. Nat. Rev. Earth Environ. 2 (8), 558–569. https://doi.org/10.1038/s43017-021-00181-9.
Gimeno, L., Nieto, R., Trigo, R.M., Vicente-Serrano, S.M., López-Moreno, J.I., 2010. Where does the Iberian Peninsula moisture come from? An answer based on a Lagrangian approach. J. Hydrometeorol. 11 (2), 421–436. https://doi.org/10.1175/2009JHM1182.1.
Hao, Z., Li, W., Singh, V.P., Xia, Y., Zhang, X., Hao, F., 2020. Impact of dependence changes on the likelihood of hot extremes under drought conditions in the United States. J. Hydrol. 581, 124410. https://doi.org/10.1016/j.jhydrol.2019.124410.
Hao, Z., Hao, F., Singh, V.P., Xia, Y., Shi, C., Zhang, X., 2018. A multivariate approach for statistical assessments of compound extremes. J. Hydrol. 565, 87–94. https://doi.org/10.1016/j.jhydrol.2018.08.025.
Hao, Z., Hao, F., Xia, Y., Feng, S., Sun, C., Zhang, X., et al., 2022. Compound droughts and hot extremes: characteristics, drivers, changes, and impacts. Earth Sci. Rev. 235, 104241. https://doi.org/10.1016/j.earscirev.2022.104241.
Hauser, M., Orth, R., Seneviratne, S.I., 2016. Role of soil moisture versus recent climate change for the 2010 heat wave in western Russia. Geophys. Res. Lett. 43 (6), 2819–2826. https://doi.org/10.1002/2016GL068036.
Hauser, M., Gudmundsson, L., Orth, R., Jézéquel, A., Haustein, K., Vautard, R., van Oldenborgh, G.J., Wilcox, L., Seneviratne, S.I., 2017. Methods and model dependency of extreme event attribution: the 2015 European drought. Earths Future 5, 1034–1043. https://doi.org/10.1002/2017EF000612.
Hersbach, H., Bell, B., Berrisford, P., Hirahara, S., Horányi, A., Muñoz-Sabater, J., et al., 2020. The ERA5 global reanalysis. Q. J. R. Meteorol. Soc. 146 (730), 1999–2049. https://doi.org/10.1002/qj.3803.
Hoffmann, D., Gallant, A.J., Arblaster, J.M., 2020. Uncertainties in drought from index and data selection. J. Geophys. Res. Atmos. 125 (18), e2019JD031946. https://doi.org/10.1029/2019JD031946.
Hong, H., Sun, J., Wang, H., 2022. Variations in summer extreme high-temperature events over northern Asia and the possible mechanisms. J. Clim. 35 (1), 335–357. https://doi.org/10.1175/JCLI-D-21-0043.1.
IPCC, 2021. In: Masson-Delmotte, V., Zhai, P., Pirani, A., Connors, S.L., Péan, C., Berger, S., Caud, N., Chen, Y., Goldfarb, L., Gomis, M.I., Huang, M., Leitzell, K., Lonnoy, E., Matthews, J.B.R., Maycock, T.K., Waterfield, T., Yelekçi, O., Yu, R., Zhou, B. (Eds.), Climate Change 2021: the Physical Science Basis. Contribution of Working Group I to the Sixth Assessment Report of the Intergovernmental Panel on Climate Change. Cambridge University Press, Cambridge, United Kingdom and New York, NY, USA, p. 2391. https://doi.org/10.1017/9781009157896.
Kam, J., Min, S.K., Wolski, P., Kug, J.S., 2021. CMIP6 model-based assessment of anthropogenic influence on the long sustained Western Cape drought over 2015–19. Bull. Am. Meteorol. Soc. 102 (1), S45–S50. https://doi.org/10.1175/BAMS-D-20-0159.1.
Kam, J., Stowers, K., Kim, S., 2019. Monitoring of drought awareness from google trends: a case study of the 2011–17 California drought. Weather, Climate, and Society 11 (2), 419–429. https://doi.org/10.1175/WCAS-D-18-0085.1.
Kautz, L.A., Martius, O., Pfahl, S., Pinto, J.G., Ramos, A.M., Sousa, P.M., Woollings, T., 2022. Atmospheric blocking and weather extremes over the Euro-Atlantic sector–a review. Weather and Climate Dynamics 3 (1), 305–336. https://doi.org/10.5194/wcd-3-305-2022.
Knutzen, F., Averbeck, P., Barrasso, C., Bouwer, L.M., Gardiner, B., Grünzweig, J.M., et al., 2025. Impacts on and damage to European forests from the 2018–2022 heat and drought events. Nat. Hazards Earth Syst. Sci. 25 (1), 77–117. https://doi.org/10.5194/nhess-25-77-2025.
Kuwayama, Y., Thompson, A., Bernknopf, R., Zaitchik, B., Vail, P., 2019. Estimating the impact of drought on agriculture using the US Drought Monitor. Am. J. Agric. Econ. 101 (1), 193–210. https://doi.org/10.1093/ajae/aay037.
Li, H., Keune, J., Gou, Q., Holgate, C.M., Miralles, D., 2024. Heat and moisture anomalies during crop failure events in the Southeastern Australian wheat belt. Earths Future 12 (3), e2023EF003901. https://doi.org/10.1029/2023EF003901.
Liu, Y., Pan, Z., Zhuang, Q., Miralles, D.G., Teuling, A.J., Zhang, T., et al., 2015. Agriculture intensifies soil moisture decline in Northern China. Sci. Rep. 5 (1), 11261. https://doi.org/10.1038/srep11261.
Liu, Y., Garcia, M., Zhang, C., Tang, Q., 2022. Recent decrease in summer precipitation over the Iberian Peninsula closely links to reduction of local moisture recycling. Hydrol. Earth Syst. Sci. 26, 1925–1936. https://doi.org/10.5194/hess-26-1925-2022.
Liu, W., Shi, N., Wang, H., Huang, Q., 2024. Thermodynamic characteristics of extreme heat waves over the middle and lower reaches of the Yangtze River Basin. Clim. Dyn. 62, 3877–3889. https://doi.org/10.1007/s00382-024-07104-6.
Lloret, F., Kitzberger, T., 2018. Historical and event-based bioclimatic suitability predicts regional forest vulnerability to compound effects of severe drought and bark beetle infestation. Glob. Change Biol. 24 (5), 1952–1964. https://doi.org/10.1111/gcb.14039.
Lorenzo, N., Díaz-Poso, A., Royé, D., 2021. Heatwave intensity on the iberian Peninsula: future climate projections. Atmos. Res. 258, 105655. https://doi.org/10.1016/j.atmosres.2021.105655.
McKee, T.B., Doesken, N.J., Kleist, J., 1993. The relationship of drought frequency and duration to time scales. Proceedings of the 8th Conference on Applied Climatology 17 (22), 179–183.
Miralles, D.G., Gentine, P., Seneviratne, S.I., Teuling, A.J., 2019. Land–atmospheric feedbacks during droughts and heatwaves: state of the science and current challenges. Ann. N. Y. Acad. Sci. 1436, 19–35. https://doi.org/10.1111/nyas.13912.
Miralles, D.G., Teuling, A.J., van Heerwaarden, C.C., Vila-Guerau de Arellano, J., 2014. Mega-heatwave temperatures due to combined soil desiccation and atmospheric heat accumulation. Nat. Geosci. 7 (5), 345–349. https://doi.org/10.1038/ngeo2141.
Mishra, A.K., Singh, V.P., 2010. A review of drought concepts. J. Hydrol. 391 (1–2), 202–216. https://doi.org/10.1016/j.jhydrol.2010.07.012.
Moemken, J., Koerner, B., Ehmele, F., Feldmann, H., Pinto, J.G., 2022. Recurrence of drought events over Iberia. Part II: future changes using regional climate projections. Tellus 74 (1), 262. https://doi.org/10.16993/tellusa.52.
Molina, M.O., Sánchez, E., Gutiérrez, C., 2020. Future heat waves over the Mediterranean from an Euro-CORDEX regional climate model ensemble. Sci. Rep. 10 (1), 8801. https://doi.org/10.1038/s41598-020-65663-0.
Mukherjee, S., Ashfaq, M., Mishra, A.K., 2020. Compound drought and heatwaves at a global scale: the role of natural climate variability-associated synoptic patterns and land-surface energy budget anomalies. J. Geophys. Res. Atmos. 125 (11), e2019JD031943. https://doi.org/10.1029/2019JD031943.
Muñoz-Sabater, J., Dutra, E., Agustí-Panareda, A., Albergel, C., Arduini, G., Balsamo, G., et al., 2021. ERA5-Land: a state-of-the-art global reanalysis dataset for land applications. Earth Syst. Sci. Data 13 (9), 4349–4383. https://doi.org/10.5194/essd-13-4349-2021.
Neumann, M., Mues, V., Moreno, A., Hassenauer, H., Seidl, R., 2017. Climate variability drives recent tree mortality in Europe. Glob. Change Biol. 23, 4788–4797. https://doi.org/10.1111/gcb.13724.
Numaguti, A., 1999. Origin and recycling processes of precipitating water over the Eurasian continent: experiments using an atmospheric general circulation model. J. Geophys. Res. 104, 1957–1972. https://doi.org/10.1029/1998JD200026.
Ojeda, M.G.V., Gámiz-Fortis, S.R., Romero-Jiménez, E., Rosa-Cánovas, J.J., Yeste, P., Castro-Díez, Y., Esteban-Parra, M.J., 2021. Projected changes in the Iberian Peninsula drought characteristics. Sci. Total Environ. 757, 143702. https://doi.org/10.1016/j.scitotenv.2020.143702.
Palmer, W.C., 1965. Meteorological drought. US. Weather Bureau Res. Paper 45, 1–58.
Papritz, L., Aemisegger, F., Wernli, H., 2021. Sources and transport pathways of precipitating waters in cold-season deep North Atlantic cyclones. J. Atmos. Sci. 78 (10), 3349–3368. https://doi.org/10.1175/JAS-D-21-0105.1.
Park, C.K., Kam, J., Byun, H.R., Kim, D.W., 2022. A self-calibrating effective drought index (scEDI): evaluation against social drought impact records over the Korean

Peninsula (1777–2020). J. Hydrol. 613, 128357. https://doi.org/10.1016/j.jhydrol.2022.128357.
Park, C.K., Byun, H.R., Deo, R., Lee, B.R., 2015. Drought prediction till 2100 under RCP 8.5 climate change scenarios for Korea. J. Hydrol. 526, 221–230. https://doi.org/10.1016/j.jhydrol.2014.10.043.
Pérez-Alarcón, A., Sorí, R., Fernández-Alvarez, J.C., Nieto, R., Gimeno, L., 2022. Where does the moisture for North Atlantic tropical cyclones come from? J. Hydrometeorol. 23 (3), 457–472. https://doi.org/10.1175/JHM-D-21-0117.1.
Pérez-Alarcón, A., Coll-Hidalgo, P., Fernández-Alvarez, J.C., Trigo, R.M., Nieto, R., Gimeno, L., 2023. Impacts of tropical cyclones on the global water budget. npj Climate and Atmospheric Science 6 (1), 212. https://doi.org/10.1038/s41612-023-00546-5.
Pérez-Alarcón, A., Sorí, R., Stojanovic, M., Vázquez, M., Trigo, R.M., Nieto, R., Gimeno, L., 2024. Assessing the increasing frequency of heat waves in Cuba and contributing mechanisms. Earth Systems and Environment 8, 1583–1599. https://doi.org/10.1007/s41748-024-00443-8.
Pérez-Alarcón, A., Fernández-Alvarez, J.C., Nieto, R., Gimeno, L., 2024. LATTIN: a Python-based tool for Lagrangian atmospheric moisture and heat tracking. Software Impacts 20, 100638. https://doi.org/10.1016/j.simpa.2024.100638.
Perkins-Kirkpatrick, S.E., Lewis, S.C., 2020. Increasing trends in regional heatwaves. Nat. Commun. 11 (1), 3357. https://doi.org/10.1038/s41467-020-16970-7.
Pisso, I., Sollum, E., Grythe, H., Kristiansen, N.I., Cassiani, M., Eckhardt, S., et al., 2019. The Lagrangian particle dispersion model FLEXPART version 10.4. Geosci. Model Dev. (GMD) 12 (12), 4955–4997. https://doi.org/10.5194/gmd-12-4955-2019.
Quandt, L.A., Keller, J.H., Martius, O., Pinto, J.G., Jones, S.C., 2019. Ensemble sensitivity analysis of the blocking system over Russia in summer 2010. Mon. Weather Rev. 147 (2), 657–675. https://doi.org/10.1175/MWR-D-18-0252.1.
Ramos, A.M., Nieto, R., Tomé, R., Gimeno, L., Trigo, R.M., Liberato, M.L., Lavers, D.A., 2016. Atmospheric rivers moisture sources from a Lagrangian perspective. Earth System Dynamics 7 (2), 371–384. https://doi.org/10.5194/esd-7-371-2016.
Ramos, A.M., Russo, A., DaCamara, C.C., Nunes, S., Sousa, P., Soares, P.M.M., et al., 2023. The compound event that triggered the destructive fires of October 2017 in Portugal. iScience 26 (3). https://doi.org/10.1016/j.isci.2023.106141.
Rios-Entenza, A., Miguez-Macho, G., 2014. Moisture recycling and the maximum of precipitation in spring in the Iberian Peninsula. Clim. Dyn. 42, 3207–3231. https://doi.org/10.1007/s00382-013-1971-x.
Rousi, E., Fink, A.H., Andersen, L.S., Becker, F.N., Beobide-Arsuaga, G., Breil, M., et al., 2023. The extremely hot and dry 2018 summer in central and northern Europe from a multi-faceted weather and climate perspective. Nat. Hazards Earth Syst. Sci. 23 (5), 1699–1718. https://doi.org/10.5194/nhess-23-1699-2023.
Russo, S., Sillmann, J., Fischer, E.M., 2015. Top ten European heatwaves since 1950 and their occurrence in the coming decades. Environ. Res. Lett. 10 (12), 124003. https://doi.org/10.1088/1748-9326/10/12/124003.
Russo, A., Gouveia, C.M., Dutra, E., Soares, P.M.M., Trigo, R.M., 2019. The synergy between drought and extremely hot summers in the Mediterranean. Environ. Res. Lett. 14 (1), 014011. https://doi.org/10.1088/1748-9326/aaf09e.
Salvador, C., Gullón, P., Franco, M., Vicedo-Cabrera, A.M., 2023. Heat-related first cardiovascular event incidence in the city of Madrid (Spain): vulnerability assessment by demographic, socioeconomic, and health indicators. Environ. Res. 226, 115698. https://doi.org/10.1016/j.envres.2023.115698.
Santos, J.A., Pfahl, S., Pinto, J.G., Wernli, H., 2015. Mechanisms underlying temperature extremes in Iberia: a Lagrangian perspective. Tellus Dyn. Meteorol. Oceanogr. 67 (1), 26032. https://doi.org/10.3402/tellusa.v67.26032.
Santos, J.A., Pinto, J.G., Ulbrich, U., 2009. On the development of strong ridge episodes over the eastern North Atlantic. Geophys. Res. Lett. 36 (17). https://doi.org/10.1029/2009GL039086.
Sánchez-Benítez, A., Barriopedro, D., García-Herrera, R., 2020. Tracking Iberian heat waves from a new perspective. Weather Clim. Extrem. 28, 100238. https://doi.org/10.1016/j.wace.2019.100238.
Sánchez-Benítez, A., García-Herrera, R., Barriopedro, D., Sousa, P.M., Trigo, R.M., 2018. June 2017: the earliest European summer mega-heatwave of reanalysis period. Geophys. Res. Lett. 45, 1955–1962. https://doi.org/10.1002/2018GL077253.
Santanello, J.A., Dirmeyer, P.A., Ferguson, C.R., Findell, K.L., Tawfik, A.B., Berg, A., Ek, M., Gentine, P., Guillod, B.P., van Heerwaarden, C., Roundy, J., 2017. Land–atmosphere interactions: the LoCo perspective. Bull. Am. Meteorol. Soc. 99 (6), 1253–1272. https://doi.org/10.1175/BAMS-D-17-0001.1.
Schumacher, D.L., Keune, J., Van Heerwaarden, C.C., Vilà-Guerau de Arellano, J., Teuling, A.J., Miralles, D.G., 2019. Amplification of mega-heatwaves through heat torrents fuelled by upwind drought. Nat. Geosci. 12 (9), 712–717. https://doi.org/10.1038/s41561-019-0431-6.
Schumacher, D.L., Keune, J., Miralles, D.G., 2020. Atmospheric heat and moisture transport to energy-and water-limited ecosystems. Ann. N. Y. Acad. Sci. 1472 (1), 123–138. https://doi.org/10.1111/nyas.14357.
Sodemann, H., Schwierz, C., Wernli, H., 2008. Interannual variability of Greenland winter precipitation sources: Lagrangian moisture diagnostic and North Atlantic Oscillation influence. J. Geophys. Res. Atmos. 113 (D3). https://doi.org/10.1029/2007jd008503.
Sousa, P.M., Barriopedro, D., Ramos, A.M., García-Herrera, R., Espírito-Santo, F., Trigo, R.M., 2019. Saharan air intrusions as a relevant mechanism for Iberian heatwaves: the ecord breaking events of August 2018 and June 2019. Weather Clim. Extrem. 26, 100224. https://doi.org/10.1016/j.wace.2019.100224.
Sousa, P.M., Trigo, R.M., Barriopedro, D., Soares, P.M., Ramos, A.M., Liberato, M.L.R., 2017. Responses of European precipitation distributions and regimes to different blocking locations. Clim. Dyn. 48, 1141–1160. https://doi.org/10.1007/S00382-016-3132-5.
Sprenger, M., Wernli, H., 2015. The LAGRANTO Lagrangian analysis tool–version 2.0. Geosci. Model Dev. (GMD) 8 (8), 2569–2586. https://doi.org/10.5194/gmd-8-2569-2015.
Stéfanon, M., Drobinski, P., D'Andrea, F., Lebeaupin-Brossier, C., Bastin, S., 2014. Soil moisture-temperature feedbacks at meso-scale during summer heat waves over Western Europe. Clim. Dyn. 42 (5–6), 1309–1324. https://doi.org/10.1007/s00382-013-1794-9.
Sutanto, S.J., Vitolo, C., Di Napoli, C., D'Andrea, M., Van Lanen, H.A., 2020. Heatwaves, droughts, and fires: exploring compound and cascading dry hazards at the pan-European scale. Environ. Int. 134, 105276. https://doi.org/10.1016/j.envint.2019.105276.
Tamarin-Brodsky, T., Hodges, K., Hoskins, B.J., Shepherd, T.G., 2020. Changes in Northern Hemisphere temperature variability shaped by regional warming patterns. Nat. Geosci. 13 (6), 414–421. https://doi.org/10.1038/s41561-020-0576-3.
Trenberth, K.E., Fasullo, J.T., 2012. Climate extremes and climate change: the Russian heat wave and other climate extremes of 2010. J. Geophys. Res. 117, D17103. https://doi.org/10.1029/11582012JD018020.
Tripathy, K.P., Mishra, A.K., 2023. How unusual is the 2022 European compound drought and heatwave event? Geophys. Res. Lett. 50 (15), e2023GL105453. https://doi.org/10.1029/2023GL105453.
Turco, M., von Hardenberg, J., AghaKouchak, A., Llasat, M.C., Provenzale, A., Trigo, R.M., 2017. On the key role of droughts in the dynamics of summer fires in Mediterranean Europe. Sci. Rep. 7 (1), 81. https://doi.org/10.1038/s41598-017-00116-9.
van der Ent, R.J., Tuinenburg, O., 2017. A. The residence time of water in the atmosphere revisited. Hydrol. Earth Syst. Sci. 21, 779–790. https://doi.org/10.5194/hess-21-779-2017.
Vázquez, M., Alvarez-Socorro, G., Fernández-Alvarez, J.C., Nieto, R., Gimeno, L., 2024. Global FLEXPART-ERA5 simulations using 30 million atmospheric parcels since 1980. Zenodo. https://doi.org/10.5281/zenodo.13682647 [Data set].
Venkatappa, M., Sasaki, N., Han, P., Abe, I., 2021. Impacts of droughts and floods on croplands and crop production in Southeast Asia–An application of Google Earth Engine. Sci. Total Environ. 795, 148829. https://doi.org/10.1016/j.scitotenv.2021.148829.
Vicente-Serrano, S.M., McVicar, T.R., Miralles, D.G., Yang, Y., Tomas-Burguera, M., 2020. Unraveling the influence of atmospheric evaporative demand on drought and its response to climate change. Wiley Interdisciplinary Reviews: Clim. Change 11 (2), e632. https://doi.org/10.1002/wcc.632.
Vicente-Serrano, S.M., Beguería, S., López-Moreno, J.I., 2010. A multiscalar drought index sensitive to global warming: the standardized precipitation evapotranspiration index. J. Clim. 23 (7), 1696–1718. https://doi.org/10.1175/2009JCLI2909.1.
Wang, W., Zhang, Y., Guo, B., Ji, M., Xu, Y., 2021. Compound droughts and heat waves over the Huai River Basin of China: from a perspective of the magnitude index. J. Hydrometeorol. 22 (11), 3107–3119. https://doi.org/10.1175/JHM-D-20-0305.1.
Wells, N., Goddard, S., Hayes, M.J., 2004. A self-calibrating palmer drought severity index. J. Clim. 17 (12), 2335–2351. https://doi.org/10.1175/1520-0442(2004)017<2335:ASPDSI>2.0.CO;2.
Wehrli, K., Luo, F., Hauser, M., Shiogama, H., Tokuda, D., Kim, H., et al., 2022. The ExtremeX global climate model experiment: investigating thermodynamic and dynamic processes contributing to weather and climate extremes. Earth System Dynamics 13, 1167–1196. https://doi.org/10.5194/esd-13-1167-2022.
Zhang, Y., Liu, C., You, Q., Chen, C., Xie, W., Ye, Z., et al., 2019. Decrease in light precipitation events in Huai River Eco-economic Corridor, a climate transitional zone in eastern China. Atmos. Res. 226, 240–254. https://doi.org/10.1016/j.atmosres.2019.04.027.
Zhang, X., Hao, Z., Singh, V.P., Zhang, Y., Feng, S., Xu, Y., Hao, F., 2022. Drought propagation under global warming: characteristics, approaches, processes, and controlling factors. Sci. Total Environ. 838, 156021. https://doi.org/10.1016/j.scitotenv.2022.156021.
Zhao, M., A, G., Velicogna, I., Kimball, J.S., 2017. A global gridded dataset of GRACE drought severity index for 2002–14: comparison with PDSI and SPEI and a case study of the Australia millennium drought. J. Hydrometeorol. 18 (8), 2117–2129. https://doi.org/10.1175/jhm-d-16-0182.1.
Zhou, S., Liang, M., Yuan, X., 2024. Impact of upwind flash drought on 2022 record-shattering heatwave over East China. Clim. Dyn. 1–14. https://doi.org/10.1007/s00382-024-07211-4.
Zhou, S., Williams, A.\P., Berg, A.M., Cook, B.I., Zhang, Y., Hagemann, S., et al., 2019. Land–atmosphere feedbacks exacerbate concurrent soil drought and atmospheric aridity. Proc. Natl. Acad. Sci. USA 116 (38), 18848–18853. https://doi.org/10.1073/pnas.1904955116.
Zhou, S., Yuan, X., 2022. Upwind droughts enhance half of the heatwaves over North China. Geophys. Res. Lett. 49 (2), e2021GL096639. https://doi.org/10.1029/2021GL096639.
Zscheischler, J., Westra, S., Van Den Hurk, B.J., Seneviratne, S.I., Ward, P.J., Pitman, A., et al., 2018. Future climate risk from compound events. Nat. Clim. Change 8 (6), 469–477. https://doi.org/10.1038/s41558-018-0156-3.
Zscheischler, J., Martius, O., Westra, S., Bevacqua, E., Raymond, C., Horton, R.M., et al., 2020. A typology of compound weather and climate events. Nat. Rev. Earth Environ. 1 (7), 333–347. https://doi.org/10.1038/s43017-020-0060-z.
Zschenderlein, P., Fragkoulidis, G., Fink, A.H., Wirth, V., 2018. Large-scale Rossby wave and synoptic-scale dynamic analyses of the unusually late 2016 heatwave over Europe. Weather 73, 275–283. https://doi.org/10.1002/wea.3278.
Zschenderlein, P., Fink, A.H., Pfahl, S., Wernli, H., 2019. Processes determining heat waves across different European climates. Q. J. R. Meteorol. Soc. 145 (724), 2973–2989. https://doi.org/10.1002/qj.3599.